Single and binary adsorption of dyes from aqueous solutions using functionalized microcrystalline cellulose from cotton fiber

Hongjuan Bai, Junhang Chen[†], Xiangyu Zhou, and Chengzhi Hu

Province Key Laboratory of Cereal Resource Transformation and Utilization, School of Chemistry and Chemical Engineering,
Henan University of Technology, Zhengzhou 450001, P. R. China

Abstract−Simultaneous removal of dyes in the effluents of printing and dyeing industries is challenging, and the mechanism of the co-adsorption of dyes is still unclear. In this context, a novel adsorbent based on microcrystalline cellulose from cotton fiber through a simplified chemical modification process was prepared. Methylene blue (MB) and neutral red (NR) were selected to investigate their adsorption/co-adsorption on such functionalized microcrystalline cellulose. The experimental adsorption results indicated that the adsorption quantity of both dyes was similar for the single solute. The kinetics of adsorption processes could be better described with the pseudo-second order models for both single and binary dye solutes. The results of the co-adsorption suggested that the extended Langmuir model could well predict equilibrium. The maximum adsorption capacity of MB and NR for the single systems was 115.2 and 83.2 mg/g, respectively. Moreover, an antagonistic effect could be found in the binary dye solute. The obtained results revealed that the co-adsorption of dyes might be driven by hydrogen bonding, π-π stacking interaction as well as electrostatic interaction.

Keywords: Dyes, Cellulose-based Adsorbent, Microcrystalline Cellulose, Adsorption Mechanism, Co-adsorption

INTRODUCTION

Currently, with the processes of industrialization, water pollution arising from organic dyes has become a global issue [1]. The existence of toxic dyes can lead to various problems such as i) affecting the transparency of water bodies, ii) retarding photosynthesis and inhibiting normal growth of autotrophic organisms, iii) causing allergy, skin irritation as well as inducing mutation of human beings, and so on [2-6]. Therefore, removing dyes from industrial effluents before they are discharged into water bodies is becoming more and more urgent [7,8]. Methylene blue (MB), a colorant and disinfector, is widely used in various industrial processes such as dyestuffs, pharmaceuticals, pesticides, rubbers and varnishes [9]. Neutral red (NR), one of the well-known cationic dyes, is a pH indicator with changing color from red to yellow over the pH range 6.8-8.0, and it has been commonly used for counterstaining nuclear in biological research [10]. The removal of MB and NR from wastewater is extremely desirable due to their toxicity.

Considerable efforts have been made to individuate the techniques for dye elimination from wastewater, which include ion exchange, flocculation, reverse osmosis, membrane processes, chemical precipitation, electrodialysis techniques and adsorption [11-17]. Among these, adsorption has been widely employed considering its advantages of high efficiency combined with low cost, simple operation, the possibility of regeneration and reusability as well as the ability to target various kinds of pollutants [18-20].

Recently, the exploitation of natural low-cost, non-toxic, cellulose based adsorbent with a dye-binding capacity for water treatment has been widely studied. These adsorbents are always derived from agro-biomass, such as sugarcane bagasse [1], banana fiber [21], rice straw [18], and oil palm fronds [22]. Cotton fiber (CF) is constituted mainly of cellulose, possessing abundant hydroxyl groups, which could be easily modified with specific functional groups (for example: cyclodextrin, amino, carboxyl as well as sulfur group) to target different types of pollutants [1]. Besides, it has been proved that cellulose could be used as an efficient adsorbent to remove organic dyes from wastewater. Microcrystalline cellulose (MCC, a white, crystalline powder and biodegradable material) with high degree of crystallinity can be isolated from α-cellulose. Compared to pristine cellulose, MCC has a lower degree of polymerization and higher surface area. Chemical modification with effective groups on cellulose and/or microcrystalline cellulose can improve adsorption ability to specific pollutants. As a widely used etherifying agent, 3-chloro-2-hydroxypropyl trimethyl ammoniumchloride (CTA) is often used for the adsorption of pollutants in wastewater treatment. Furthermore, 2-acrylamide-2-methyl propane sulfonic acid (AMPS), as a water treatment agent, has been used for the adsorption of cationic pollutants.

So far, the utilization of cotton fiber as adsorbent for organic dyes removal from aqueous solutions has been reported [23]; however, little research has been focused on the application of microcrystalline cellulose from cotton fiber used as adsorbent for organic dye elimination. Additionally, many researchers have only focused on the adsorption of organic dyes onto the cellulose-based adsorbents in single-component aqueous system; to our knowledge there has been no report concerning the usage of MCC from CF for dye removal in the co-adsorption of dye system. In fact, there are multiple components of dyes in real drainage waters, and

[†]To whom correspondence should be addressed.
E-mail: chenjunhang@haut.edu.cn

the coexistence of the multiplicity may have interactive effects that can affect the behavior of dye adsorption.

Therefore, in this work, we synthesized a novel adsorbent based on microcrystalline cellulose (MCC) from cotton fiber (CF) via a simplified and effective chemical modification process for dyeing wastewater treatment. The cellulose-based adsorbent was obtained by grafting CTA and AMPS on microcrystalline cellulose from cotton fiber. The resulting functionalized microcrystalline cellulose (FMCC) was used to capture methylene blue (MB) and neutral red (NR) via a batch process in a single and binary systems. Various experimental techniques namely scanning electron microscopy (SEM), Fourier transform infrared spectrometry (FTIR), powder X-ray diffraction (XRD) and the specific surface area, pore volume and pore size distribution were used to characterize the structure and morphology of the obtained adsorbent. The adsorption of kinetics and multi-component isotherms was investigated to reveal the binding mechanism and interactions between dyes and adsorbent. The obtained results provide reliable scientific basis in practical application for dye removal.

MATERIALS AND METHODS

1. Preparation of Functionalized Microcrystalline Cellulose (FMCC) and Its Physicochemical Characterization

The FMCC was prepared according to an adaptation of the methodology described by Xiong et al. [23]. Briefly, the cotton fibers (10.0 g) were cut into small segments (about 5 mm) and then put into 2 wt% NaOH solution (500 mL) for 2 h. Then the fibers above were neutralized by sulfuric acid and washed thoroughly with pure water. After drying at 60 °C for 4 h, the obtained fibers were immersed into 8 wt% H_2SO_4 solution (300 mL) with continuous stirring for 2 h at 80 °C, which facilitated the hydrolysis. Then, the above mixture was neutralized by NaOH solution and washed thoroughly. After drying at 60 °C for 4 h, the microcrystalline cellulose (MCC) was obtained.

Then 8.0 g MCCs and 16.0 g CTA with 6.0 mL NaOH solution (10 wt%) were added into 80 mL acetone, and the mixture was stirred 45 °C for 3 h, then neutralized, filtered and washed thoroughly; and after drying at 90 °C for 1 h, the obtained product (5.0 g) was suspended into distilled water (200 mL) under continuous stirring and 10.0 g $Ce(NH_4)_2(NO_3)_6$ was put into the above system. After 30 min stirring, 15.0 g AMPS was put subsequently into the system above for 4 h. The resultant mixture was followed by filtering, washing thoroughly and drying at 60 °C for 4 h. Finally, the functionalized microcrystalline cellulose (FMCC, a yellow solid product) was obtained. All reactants used in this work, which were purchased from Aladdin®, were of analytical grade. The physicochemical properties of MCC and FMCC were characterized by SEM, FTIR, XRD as well as the specific surface area, pore volume and pore size distribution.

2. Experiments of Adsorption

Batch adsorption experiments were performed to investigate the isotherms and kinetics for MB and NR adsorption by FMCC in single and binary dye solutes.

2-1. Adsorption Equilibrium Isotherms

For adsorption isotherm study, an optimized dosage of 2.5 g/L

of FMCC was added into the solution with varying MB or NR concentration (50 mg/L to 500 mg/L). After adsorption, the NR concentration in the supernatant was determined at λ_{max} 525 nm and MB was measured at λ_{max} 665 nm, respectively, by a spectrophotometer (PUXI TU1800).

With regard to the co-adsorption of MB and NR, the dye solution for adsorption isotherms was prepared as follows: the target dye varying at different concentrations with the concentration of interferential dye was fixed [19]. One set of experiments was conducted varying MB concentrations from 20 mg/L to 500 mg/L while selecting NR concentration fixed at 50 mg/L (or 100 mg/L, or 200 mg/L). The other set of experiments was carried out selecting NR concentration varying from 20 mg/L to 500 mg/L while the MB concentration was fixed at 50 mg/L (or 100 mg/L, or 200 mg/L).

All tests were performed at 298K with constant agitation (150 rpm) and without pH adjustment. The dye concentrations of MB (C_A) and NR (C_B) in the co-adsorption solution were measured as follows [24]:

$$C_A = \frac{k_{B2}A_1 - k_{B1}A_2}{k_{A1}k_{B2} - k_{A2}k_{B1}} \tag{1}$$

$$C_B = \frac{k_{A1}A_2 - k_{A2}A_1}{k_{A1}k_{B2} - k_{A2}k_{B1}} \tag{2}$$

where k_{A1}, k_{B1}, k_{A2} and k_{B2} refer to calibration constants of dye A and dye B at $\lambda_{1,max}$ and $\lambda_{2,max}$, respectively. A_1 and A_2 represent the values of absorbance measured at $\lambda_{1,max}$ and $\lambda_{2,max}$, respectively.

The adsorption amount of dye (q_e) and the decreasing ratio (Dr) were determined as follows:

$$q_e = \frac{V(C_0 - C_e)}{m} \tag{3}$$

$$Dr = \frac{q_e - q_e'}{q_e} \times 100\% \tag{4}$$

where C_0 refers to the initial dye concentration (mg/L) and C_e represents the equilibrium dye concentration (mg/L); m refers to the mass of adsorbent (g); V (L) refers to the solution volume; q_e represents the equilibrium adsorption capacity (mg/g); Dr refers to the decreasing ratio after inducing the interferential dye and q_e' refers to the equilibrium adsorption quantity (mg/g) in co-adsorption systems.

2-2. Mathematical Models for Adsorption Isotherms

For the single dye system, the equilibrium data was interpreted by Langmuir model [25]:

$$q_e = \frac{q_m K_L C_e}{1 + K_L C_e} \tag{5}$$

where C_e refers to the equilibrium dye concentration (mg/L), q_e and q_{max} refer to the equilibrium adsorption capacity and the estimated maximum monolayer adsorption quantity of dye (mg/g), respectively, and K_L is the constant of the model (L/mg).

Q_b/Q_s could be used to evaluate the interaction of two components in binary mixtures, where Q_b and Q_s refer to the adsorption quantity of dye in binary and single system, respectively. Three types of effects exist in the multi-component system: synergism, antagonism and non-interaction [26]:

i) When $Q_b/Q_s > 1$, it is the synergism effect, which means the effect of the component in the binary mixtures is larger than the individual effect of the component;

ii) When $Q_b/Q_s < 1$, it is the antagonism effect, which means the effect of the component in the binary mixtures is smaller than the individual effect of the component;

iii) When $Q_b/Q_s = 1$, there is non-interaction, which means the effect of the component in the binary mixtures is as much as the individual effect of the component.

In this study, the extended Langmuir isotherm was employed to interpret equilibrium data for the binary system [27].

For MB:

$$q_{e,1} = \frac{q_{m,1}K_{L,1}C_{e,1}}{1 + K_{L,1}C_{e,1} + K_{L,2}C_{e,2}} \tag{6}$$

For NR

$$q_{e,2} = \frac{q_{m,2}K_{L,2}C_{e,2}}{1 + K_{L,2}C_{e,2} + K_{L,1}C_{e,1}} \tag{7}$$

where 1 and 2 (the subscripts) refer to MB and NR, respectively.

2-3. Kinetics Study of the Adsorption

The effect of contact time was investigated with 0.025 g of adsorbent and 10 mL initial concentration of MB or NR at 200 mg/L in the 50 mL conical flasks and agitation in a shaker at fixed speed of 150 rpm. Then the flasks were taken out of the shaker at a given time to measure the concentration of the dye. For the binary system of MB and NR, with the same adsorbent dosage and initial concentrations (200 mg/L) as in single system addressed above, the total initial concentrations of MB and NR were kept with the ration fixed at 1 : 1. And the procedure for analysis was also the same as described above for adsorption isotherm experiments.

2-4. Adsorption Kinetic Models used in this Study

Three models--the pseudo-first order (PFO), pseudo-second order (PSO) and Avrami models--were used to evaluate the kinetics of adsorption by fitting the experimental curves. The expressions of PFO, PSO and Avrami models are given as follows [24]:

The pseudo-first-order equation: $q_t = q_e(1 - e^{-k_1 t})$ (8)

The pseudo-second-order equation: $q_t = \dfrac{k_2 q_e^2 t}{1 + k_2 q_e t}$ (9)

The Avrami model: $q_t = q_e(1 - e^{(-k_{av}t)^n})$ (10)

where q_e and q_t refer to the dye adsorption quantity (mg/g) at equilibrium and at time t (min), respectively; and k_1, k_2 and k_{av} represent the adsorption rate constant of PFO (1/min), PSO (g/mg·min) and Avrami (1/min) models, respectively.

3. Model Validation

Marquardt's percent standard deviation (MPSD) was employed to evaluate the experimental data of adsorption equilibrium, which was described by the following eq. [28]:

$$MPSD = 100 \times \sqrt{\frac{1}{N-P} \sum \left(\frac{q_{e,i}^{exp} - q_{e,i}^{cal}}{q_{e,i}^{exp}} \right)^2}$$

where $q_{e,i}^{exp}$ is the experimental specific adsorption quantity (mg/g), $q_{e,i}^{cal}$ is the calculated specific adsorption quantity (mg/g) which cor-

responds to $q_{e,i}^{exp}$, N refers to the experimental observation number and P refers to the parameter numbers in the regression model.

The statistical index of Average Relative Error (ARE) was employed to validate the goodness of fit of kinetic adsorption data, and the expression of ARE was described below [28]:

$$ARE(\%) = \frac{100}{N} \times \sqrt{\sum \left(\frac{q_{e,i}^{exp} - q_{e,i}^{cal}}{q_{e,i}^{exp}} \right)^2}$$

Smaller values of ARE suggest more accurate value of q_t.

RESULTS AND DISCUSSION

1. Adsorbent Characterization

The SEM of raw cotton, microcrystalline cellulose (MCC) and functionalized microcrystalline cellulose (FMCC) are given in Fig. 1. The raw cotton surface was smooth and there was no wrinkle on it (Fig. 1(a)). MCC (Fig. 1(b)) revealed a rough surface with few wrinkles along the fiber strands compared to that of raw cotton (Fig. 1(a)). However, after chemical treatment, the surface morphology of FMCC (Fig. 1(c)) was much rougher and some tablet shapes could be found on it. Consequently, this may be attributed to excellent adsorption property of FMCC, and better adsorption of dyes by the FMCC is expected.

FTIR analyses showed that the spectra of FMCC were comparable to that of MCC. The wide absorption peak at ~3,400 cm^{-1} was related to -OH groups, and the band at ~2,900 cm^{-1} was caused by -CH$_2$ groups stretching. The absorption peak at 1,430 cm^{-1} corresponded to bending vibration of a symmetric CH$_2$, which is known as the crystallinity band [22]. The absorption band at ~1,165 cm^{-1} was due to C-O-C stretching. The absorption band at 1,238 cm^{-1} would correspond to C-O groups stretching, which was absent with the process of modification. This indicated that hydrogen bonding between the hydroxyl groups of cellulose was reduced in inter- or intramolecular after modification [23]. The presence of peaks at 1,647 cm^{-1} and 1,552 cm^{-1} would be caused by amide I ($v_{C=O}$) amide II (δ_{N-H}), respectively, which confirmed that the amide group was introduced to FMCC after modification.

The crystalline structure of the adsorbents is essential for the performance of adsorption. Fig. 1(e) displays the XRD patterns of the MCC and FMCC. From the figure, the diffraction peaks at 22.5°, 14.5° and 34.6° correspond to the 101, 002 and 040 crystal planes of cellulose [29], respectively. The diffraction peaks of FMCC were less intense than MCC, indicating that the intra- and intermolecular hydrogen bonds of MCC might be rearranged with the process of modification. Such results are in consistent with the results obtained from FTIR.

The specific surface and area and pore size distribution of FMCC were measured with NOVA 1000 High-Speed Automated Surface Area and Pore Size Analyzer (American), and the BET adsorption model was used in the calculation. Calculation of pore size followed the method of BJH according to the implemented software routines. The surface area and pore size distribution of FMCC were revealed by N$_2$ adsorption-desorption measurements (Fig. 1(f)). The BET surface area of FMCC was calculated to be 8.32 m^2/g. The pore volume and average pore diameter of FMCC were

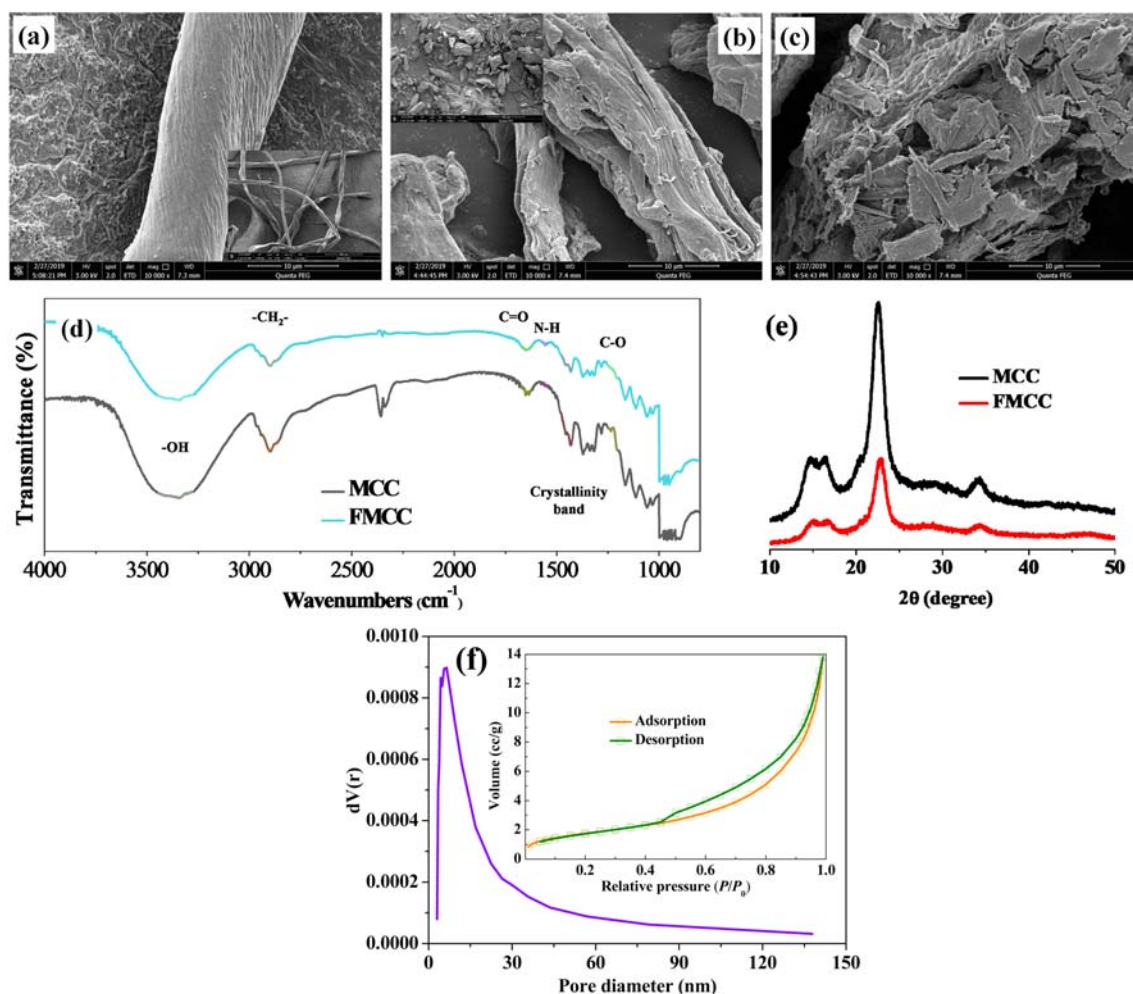**Fig. 1. Characterization of MCC and FMCC: (a, b, c) SEM, (d) FTIR, (e) XRD and (f) pore size distribution and N2 sorption isotherm (insert) of FMCC.**

0.021 cm^3/g and 6.44 nm, respectively. This shows that FMCC is reasonably good for adsorption.

2. Adsorption Equilibrium Studies

The equilibrium curves of MB and NR adsorption onto FMCC in mono-component and co-adsorption systems were observed with concentrations varying from 20 to 500 mg/L (Fig. 2). And the equilibrium data of MB and NR fitted by Langmuir model and extended Langmuir model for the mono-component and co-adsorption systems, respectively. The parameters of adsorption isotherm obtained from both models are shown in Table 1. The experimental data can be well fitted by both models (R^2>0.969, Table 1). From Table 1, the q_m values of MB are higher than those of NB in single dye system. The calculated Q_b/Q_s values for both MB and NR are smaller than 1 (Table 1), suggesting that antagonism effect occurred in the binary dye adsorption processes [1].

From Table 1 and Fig. 2, for both MB and NR, the adsorption capacity of dyes in the co-adsorption system was lower than those in mono-component solute. Besides, the adsorption capacity of the target dye was decreased with the interferential dye concentration increasing, especially in the higher concentration. For MB, the value of q_{max} was 115.2 mg/g in single dye solution, while it decreased

to 77 mg/g with the coexistence of 200 mg/L NR (Fig. 2 and Table 1), and the decreasing ration was about 33%. Antagonistic effect between both dyes was found for MB adsorption on FMCC in the presence of fixed concentrations of NR. Similar results were also observed when NR was the target dye. The value of q_{max} was 83.2 mg/g in single NR solution, while it decreased to 64 mg/g in the presence of 200 mg/L MB with a decreasing ration of 23% (Fig. 2 and Table 1). The K_L values for MB were decreased with the interferential dye NR concentration increasing (from 50 mg/L to 200 mg/L) (Table 1), due to a high adsorption affinity between dyes and FMCC at the lowest initial concentration of the interferential dye (50 mg/L NR) in the binary dye system. Similar tendency of K_L values for NR was observed (Table 1). This suggested that the adsorption affinity of the target dye to FMCC was influenced by the coexistence of the interferential dye in the binary systems for both MB and NR. Such antagonism between the two dyes could be explained by competitive adsorption phenomena on the active adsorption sites [30].

The 3D adsorption surfaces for adsorption capacity of the target dye against the equilibrium concentrations at three concentrations of the target dye (50 mg/L, 100 mg/L and 200 mg/L) are

Table 1. Isotherm parameters of adsorption of MB and NR onto FMCC in single and binary dye solution

|		For MB				For NR		
Single system	q_m (mg/g)	115.16±3.14			q_m (mg/g)	83.19±1.45		
	K_L (L/mg)	0.131±0.015			K_L (L/mg)	0.167±0.015		
	R^2	0.974			R^2	0.986		
	MPSD	39.86			MPSD	9.97		
		For MB				**For NR**		
	Parameters	$C_{0,NR}$/(mg/L)			Parameters	$C_{0,MB}$/(mg/L)		
		50	100	200		50	100	200
Binary system	q_m (mg/g)	100.24±4.22	86.78±5.82	76.95±3.29	q_m (mg/g)	76.70±8.58	66.16±6.45	63.64±7.96
	K_L (L/mg)	0.021±0.003	0.017±0.002	0.0068±0.001	K_L (L/mg)	0.089±0.028	0.0564±0.019	0.0520±0.014
	K_{L-NR} (L/mg)	−0.122±0.01	−0.0727±0.009	−0.0198±0.001	K_{L-MB} (L/mg)	0.0596±0.01	−0.0023±0.001	−0.164±0.043
	R^2	0.994	0.993	0.995	R^2	0.966	0.972	0.969
	Q_b/Q_s	0.870	0.754	0.668	Q_b/Q_s	0.922	0.795	0.765
	MPSD	7.08	6.73	3.99	MPSD	15.51	10.23	18.09
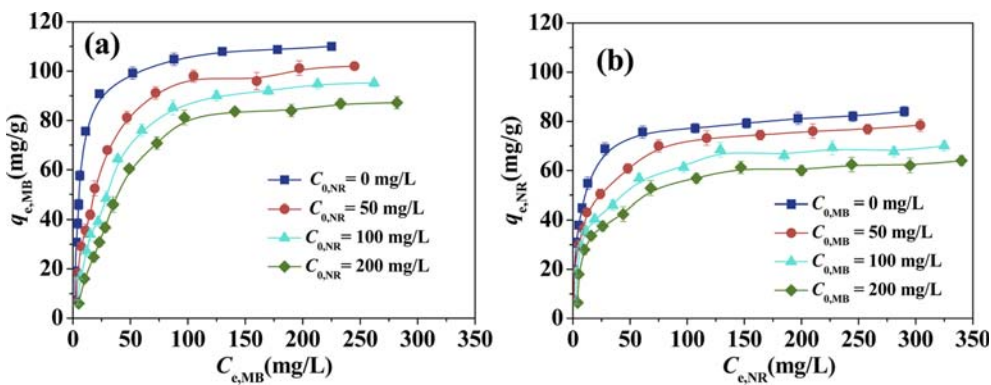
Fig. 2. Equilibrium curves for the adsorption of MB (a) and NR (b) onto FMCC in single (blue color) and binary systems (red, cyan, green color).
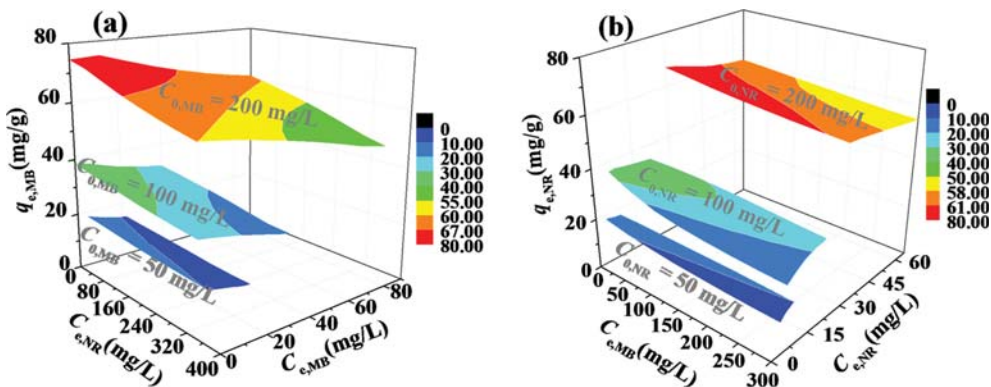

Fig. 3. Three-dimensional isotherm surfaces of MB-NR adsorption binary system onto FMCC. (a) The adsorption capacity of MB is plotted as a function of the equilibrium concentrations of MB and NR; (b) The adsorption capacity of NR is plotted as a function of the equilibrium concentrations of NR and MB.

shown in Fig. 3. As indicated by the even 3D surface of adsorption, both MB and NR dyes could interfere in the adsorption of each other (Fig. 3). For MB, with the MB concentration increasing (50 mg/L, 100 mg/L and 200 mg/L), the q_{max} value (18.4, 38.8 and 75.7 mg/g) and the decreasing ratio (53.6%, 58.8% and 67.4%) of MB were increasing (Fig. 3(a)). Similar tendency was obtained

for NR from the adsorption surface (Fig. 3(b)). When NR concentration increased at 50, 100 and 200 mg/L, the q_{max} of NR was 18.6, 37.6 and 67.6 mg/g and the decreasing ratio value of NR was about 12.9%, 18.8% and 23.9%, respectively. Compared to the decreasing ratio of both dyes, the presence of NR had a stronger effect on the adsorption of MB in the co-adsorption solutes.
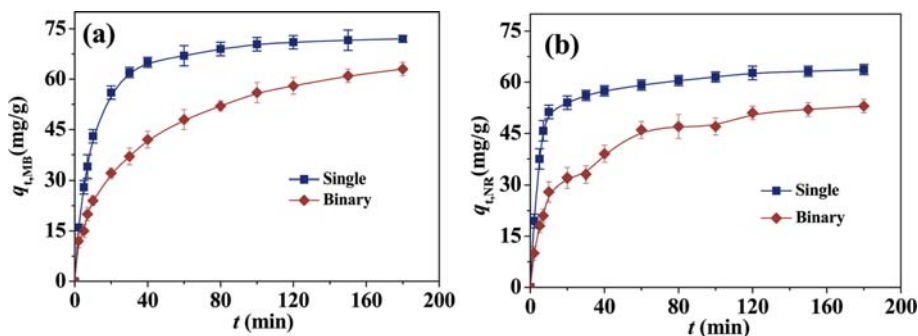
Fig. 4. Kinetic curves for the dye adsorption of MB (a) and NR (b) on FMCC in single and binary systems.

Table 2. Kinetic parameters for the adsorption of MB and NR onto FMCC in single and binary systems

Kinetic model	MB		NR	
	Single	Binary	Single	Binary
Pseudo-first-order equation				
q_t (mg/g)	69.22±0.89	57.08±2.15	60.09±0.86	48.23±1.81
k_1 (1/min)	0.095±0.005	0.040±0.005	0.194±0.014	0.064±0.009
R^2	0.991	0.956	0.983	0.936
ARE (%)	5.63	19.79	6.53	19.48
Pseudo-second-order equation				
$k_2 \times 10^3$ (g/mg·min)	1.67±0.07	0.73±0.10	4.53±0.42	1.55±0.23
q_t (mg/g)	76.09±0.58	67.17±2.09	63.96±0.83	54.18±1.54
R^2	0.998	0.984	0.990	0.978
ARE (%)	1.23	7.11	3.86	6.57
Avrami model				
q_{av} (mg/g)	69.23±0.93	57.79±2.25	60.08±0.90	48.24±1.89
k_{av} (1/min)	0.081±0.005	0.051±0.002	0.24±0.008	0.080±0.003
n	1.17±0.045	0.78±0.024	0.81±0.039	0.79±0.005
R^2	0.991	0.956	0.983	0.936
ARE (%)	6.14	21.59	7.12	21.25

3. Kinetics Studies of Adsorption

Information on the kinetic behavior (adsorption capacity versus time) of MB and NR adsorption onto FMCC in both mono-component and co-adsorption systems with the same concentrations (200 mg/L) is provided in Fig. 4. From Fig. 4, at the same concentrations, the q_{max} in the mono-component solute was higher than that in co-adsorption systems for MB and NR. Besides, the q_{max} of MB was higher than that of NR in both mono-component and co-adsorption of dye solutes. The reduction of q_{max} in binary systems indicated the interference of each other for MB and NR. To obtain the kinetic parameters (Table 2), the experimental data were fitted by the three models (PFO, PSO and Avrami). From Table 2, the pseudo-second order model (PSO) was the most suitable for interpreting observations from the experiments in both mono-component and co-adsorption solutes (R^2>0.978 and ARE <7.2%), suggesting that the adsorption rate was chemical sorption [31]. Moreover, for both dyes, the value of k_2 in single solutes was higher than that in binary solutes, suggesting that faster dye adsorption occurred in single systems compared to binary contaminated systems, which was in agreement with the results obtained from
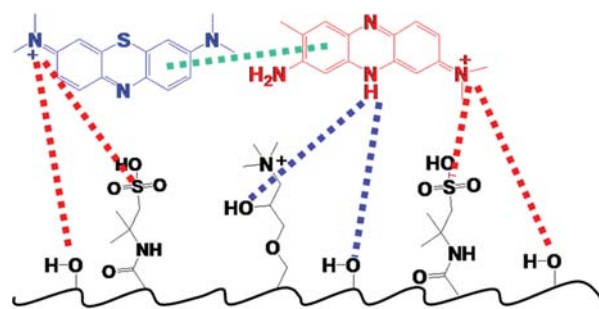

Fig. 5. Adsorption mechanism: electrostatic attractions (red color), hydrogen bonds (blue color), and π-π stacking interactions (green color).

Fig. 4; more time is required to achieve equilibrium for the binary system. Similar results were also obtained by other authors [19].

4. Possible Adsorption Mechanism Analysis

In this work, the plausible adsorption mechanisms of dyes onto FMCC were mainly associated with hydrogen bonding, π-π stacking and electrostatic interaction (Fig. 5): (i) When in the solution,

MB/NR has a net positive charge [32], which can form electrostatic attraction with the surface of adsorbents, which have numerous functional groups (especially oxygen-containing groups). Besides, after modification, there are some groups of SO_3^{2-} on the surface of the FMCC which can provide negatively charge for adsorption of cationic dyes (MB and NR). (ii) Hydrogen bonding could be formed via the N^+ of MB or NR and the -OH of the adsorbents [32,33]. (iii) In the co-adsorption system, the benzene rings in the MB and NR molecules could form the π-π stacking interaction, and the specific sites on the surface of the adsorbents could be partially overlapped with MB and NR due to the competitive adsorption of both dyes.

CONCLUSIONS

Cellulose-based bioadsorbent (FMCC) was obtained by grafting CTA and AMPS on microcrystalline cellulose from cotton fiber. Simultaneous adsorption processes of MB and NR on FMCC from binary system were investigated. For the co-adsorption solute, the extended Langmuir model well described the adsorption isotherms of both dyes. Kinetic studies suggested that PSO model was the most suitable and chemisorption could be the adsorption mechanism. And the processes of adsorption were driven by hydrogen bonding, π-π stacking and electrostatic interaction. This study shows that FMCC could be a good candidate to remove organic dyes from binary systems. Nevertheless, further experiments need to be performed on how to recycle the adsorbent.

ACKNOWLEDGEMENTS

REFERENCES

1. F. Wang, Y. Pan, P. Cai, T. Guo and H. Xiao, *Bioresour. Technol.*, **241**, 482 (2017).
2. F. M. Mpatani, A. A. Aryee, A. N. Kani, Q. Guo, E. Dovi, L. Qu, Z. Li and R. Han, *Chemosphere*, **259**, 127439 (2020).
3. S. N. Jain, S. R. Tamboli, D. S. Sutar, S. R. Jadhav, J. V. Marathe, A. A. Shaikh and A. A. Prajapati, *J. Clean. Prod.*, **252**, 119778 (2020).
4. W. Xiao, Z. N. Garba, S. Sun, I. Lawan, L. Wang, M. Lin and Z. Yuan, *J. Clean. Prod.*, **253**, 119989 (2020).
5. M. A. Islam, I. Ali, S. M. A. Karim, M. S. Hossain Firoz, A.-N. Chowdhury, D. W. Morton and M. J. Angove, *J. Water Process Eng.*, **32**, 100911 (2019).
6. F. C. Çavuşoğlu, S. Akan, E. A. Arı, E. Çetinkaya, E. Çolak, G. N. Daştan, S. Deniz, D. Erdem, M. Köksal, S. Korkmaz, N. Onsekiz, B. Oruçoğlu, D. Özkaya, H. B. Uslu, Ç. Ünal, O. Yıldız, Ş. Özkara-Aydınoğlu and Ş. S. Bayazit, *Korean J. Chem. Eng.*, **36**, 1915 (2019).
7. G. D. Değermenci, N. Değermenci, V. Ayvaoğlu, E. Durmaz, D. Çakır and E. Akan, *J. Clean. Prod.*, **225**, 1220 (2019).
8. M. Sarabadan, H. Bashiri and S. M. Mousavi, *Korean J. Chem. Eng.*, **36**, 1575 (2019).
9. B. Chen, H. Zhao, S. Chen, F. Long, B. Huang, B. Yang and X. Pan, *Chem. Eng. J.*, **356**, 69 (2019).
10. Q. Zhou, W. Gong, C. Xie, D. Yang, X. Ling, X. Yuan, S. Chen and X. Liu, *J. Hazard. Mater.*, **185**, 502 (2011).
11. D. Humelnicu, M. M. Lazar, M. Ignat, I. A. Dinu, E. S. Dragan and M. V. Dinu, *J. Hazard. Mater.*, **381**, 120980 (2020).
12. Y. Pan, H. Xie, H. Liu, P. Cai and H. Xiao, *Bioresour. Technol.*, **286**, 121366 (2019).
13. E. F. Diogo Januário, N. de Camargo Lima Beluci, T. B. Vidovix, M. F. Vieira, R. Bergamasco and A. M. Salcedo Vieira, *Process Saf. Environ. Prot.*, **134**, 140 (2020).
14. N. C. Homem, N. de Camargo Lima Beluci, S. Amorim, R. Reis, A. M. S. Vieira, M. F. Vieira, R. Bergamasco and M. T. P. Amorim, *Appl. Surf. Sci.*, **486**, 499 (2019).
15. N. Ghaemi and P. Safari, *J. Hazard. Mater.*, **358**, 376 (2018).
16. A. S. Abdulhameed, A.-T. Mohammad and A. H. Jawad, *J. Clean. Prod.*, **232**, 43 (2019).
17. H. Bashiri, S. Nesari and M. Sarabadan, *Korean J. Chem. Eng.*, **37**, 240 (2020).
18. Q. Liu, Y. Li, H. Chen, J. Lu, G. Yu, M. Möslang and Y. Zhou, *J. Hazard. Mater.*, **382**, 121040 (2020).
19. E. K. Shirazi, J. W. Metzger, K. Fischer and A. H. Hassani, *Chemosphere*, **234**, 618 (2019).
20. D. Yu, Y. Wang, M. Wu, L. Zhang, L. Wang and H. Ni, *J. Clean. Prod.*, **232**, 774 (2019).
21. K. Vijayalakshmi, B. M. Devi, S. Latha, T. Gomathi, P. N. Sudha, J. Venkatesan and S. Anil, *Int. J. Biol. Macromol.*, **104**, 1483 (2017).
22. M. H. Hussin, N. A. Pohan, Z. N. Garba, M. J. Kassim, A. A. Rahim, N. Brosse, M. Yemloul, M. R. N. Fazita and M. K. M. Haafiz, *Int. J. Biol. Macromol.*, **92**, 11 (2016).
23. J. Q. Xiong, C. L. Jiao, C. M. Li, D. S. Zhang, H. Lin and Y. Y. Chen, *Cellulose*, **21**, 3073 (2014).
24. J. O. Gonçalves, K. A. da Silva, E. C. Rios, M. M. Crispim, G. L. Dotto and L. A. de Almeida Pinto, *Int. J. Biol. Macromol.*, **142**, 85 (2020).
25. Y. Rong and R. Han, *Korean J. Chem. Eng.*, **36**, 942 (2019).
26. E. A. Mohamed, A. Q. Selim, S. A. Ahmed, L. Sellaoui, A. Bonilla-Petriciolet, A. Erto, Z. Li, Y. Li and M. K. Seliem, *Chem. Eng. J.*, **380**, 122445 (2020).
27. M. A. Hossain, H. H. Ngo, W. S. Guo, L. D. Nghiem, F. I. Hai, S. Vigneswaran and T. V. Nguyen, *Bioresour. Technol.*, **160**, 79 (2014).
28. B. Agarwal, C. Balomajumder and P. K. Thakur, *Chem. Eng. J.*, **228**, 655 (2013).
29. Q. Chen, J. Zheng, L. Zheng, Z. Dang and L. Zhang, *Chem. Eng. J.*, **350**, 1000 (2018).
30. L. J. Li, F. Q. Liu, X. S. Jing, P. P. Ling and A. M. Li, *Water Res.*, **45**, 1177 (2011).
31. N. Deihimi, M. Irannajad and B. Rezai, *J. Environ. Manage.*, **227**, 277 (2018).
32. B. Wang, Y. B. Zhai, T. F. Wang, S. H. Li, C. Peng, Z. X. Wang, C. T. Li and B. B. Xu, *Bioresour. Technol.*, **274**, 525 (2019).
33. Z. B. Wu, H. Zhong, X. Z. Yuan, H. Wang, L. L. Wang, X. H. Chen, G. M. Zeng and Y. Wu, *Water Res.*, **67**, 330 (2014).